

## Tropical Clouds and Circulation Changes during the 2006/07 and 2009/10 El Niños

HUI SU AND JONATHAN H. JIANG

*Jet Propulsion Laboratory, California Institute of Technology, Pasadena, California*

(Manuscript received 2 March 2012, in final form 27 June 2012)

### ABSTRACT

Changes in tropical cloud vertical structure, cloud radiative forcing (CRF), and circulation exhibit distinctly different characteristics during the 2006/07 and 2009/10 El Niños, revealed by *CloudSat* and *Cloud–Aerosol Lidar and Infrared Pathfinder Satellite (CALIPSO)* observations and reanalysis data. On the tropical average, the 2009/10 has a decrease of clouds from 2 to 14 km, an increase of clouds in the boundary layer, and an increase of cirrus clouds above 14 km. The tropical-mean cloud anomalies in the middle to upper troposphere (6–14 km) for the 2006/07 El Niño are nearly opposite to those in 2009/10 El Niño. The tropical averaged net CRF anomaly at the top of the atmosphere (TOA) is  $0.6\text{--}0.7 \text{ W m}^{-2}$  cooling ( $0.02\text{--}0.5 \text{ W m}^{-2}$  warming) for the 2009/10 (2006/07) El Niño. The 2009/10 El Niño is associated with a strengthening of tropical circulation, increased high (low) clouds in extremely strong ascending (descending) regimes, and decreased clouds in the middle and high altitudes in a broad range of moderate circulation regimes. The strengthening of tropical circulation is primarily caused by the enhancement of the Hadley circulation. The 2006/07 El Niño is associated with a weakening of the tropical circulation, primarily caused by the reduction of the Walker circulation. The cloud anomalies in each circulation regime are approximately opposite for these two El Niños. The analysis herein suggests that both the magnitude and pattern of sea surface temperature anomalies in the two events contribute to the differences in clouds and circulation anomalies, with magnitude playing a dominant role. The contrasting behaviors of the two El Niños highlight the nonlinear response of tropical clouds and circulation to El Niño SST forcing.

### 1. Introduction

On interannual time scales, El Niño–Southern Oscillation (ENSO) is the most dominant natural variability. ENSO is characterized by anomalous sea surface temperature (SST) in the equatorial Pacific and has far-reaching impacts on global and regional temperature, precipitation, and circulation. Changes in tropical clouds during ENSO have been studied extensively (e.g., Ramanathan and Collins 1991; Zhang et al. 1996; Cess et al. 2001; Allan et al. 2002) owing to the profound importance of clouds on the earth's radiative energy balance. At the time when no direct observation of cloud vertical profiles on the tropical/global scale was available, a few studies used the ratio of shortwave and longwave cloud forcing (SWCF and LWCF, respectively) at the top of the atmosphere (TOA),  $N = -\text{SWCF}/\text{LWCF}$ , to infer cloud height for the understanding of TOA

cloud radiative forcing (CRF) changes. There has been a controversy as to whether the abnormally large  $N$  value over the western Pacific warm pool during the 1998 El Niño was dominated by lowering of deep convective cloud heights (Cess et al. 2001) or increasing low-level clouds associated with anomalous subsidence (Allan et al. 2002). Yuan et al. (2008) revisited the issue by analyzing the International Satellite Cloud Climatology Project (ISCCP) cloud fraction data along with the CRF estimates from the Earth Radiation Budget Experiment (ERBE) and the Clouds and the Earth's Radiant Energy System (CERES) as a function of large-scale vertical motion, following the methodology put forward by Bony et al. (2004). Their results showed that both high and low clouds underwent significant changes during the 1998 El Niño and the shift from “top-heavy” to “bottom-heavy” upward motion in the western Pacific appeared to be responsible for the cloud vertical structure change, rather than the mean vertical motion.

*CloudSat* and *Cloud–Aerosol Lidar and Infrared Pathfinder Satellite (CALIPSO)* experiments have conducted global survey of cloud vertical profiles since 2006. These measurements enable us to unambiguously identify

Corresponding author address: Hui Su, Jet Propulsion Laboratory, California Institute of Technology, 4800 Oak Grove Drive, Pasadena, CA 91109.  
E-mail: hui.su@jpl.nasa.gov

changes of cloud vertical structure in response to El Niño. During the *CloudSat/CALIPSO* observational period, two El Niños occurred. Based on the difference in the SST anomalies averaged over the Niño-4 ( $5^{\circ}\text{S}$ – $5^{\circ}\text{N}$ ,  $160^{\circ}\text{E}$ – $150^{\circ}\text{W}$ ) and Niño-3 ( $5^{\circ}\text{S}$ – $5^{\circ}\text{N}$ ,  $150^{\circ}$ – $90^{\circ}\text{W}$ ) regions, the two El Niños were classified as two different types of El Niño (Yeh et al. 2009; Lee and McPhaden 2010; Yu and Kim 2012). The 2006/07 El Niño was a moderate eastern Pacific El Niño (EP-El Niño), characterized by warm SST anomalies across the eastern and central Pacific with a Niño-3 SST anomaly greater than that over Niño-4. In contrast, the winter of 2009/10 experienced large positive SST anomalies over the central Pacific with a Niño-4 SST anomaly significantly higher than Niño-3, making it the strongest central Pacific El Niño (CP-El Niño) since the 1980s (Lee and McPhaden 2010). The CP-El Niño is also called El Niño Modoki and is associated with different, even opposite, teleconnection patterns from the canonical EP-El Niño (Latif et al. 1997; Ashok et al. 2007; Kao and Yu 2009; Kug et al. 2009; Weng et al. 2007; Weng et al. 2009; Kim et al. 2009). We note that the magnitude of the 2006/07 El Niño is much weaker than that of the 1997/98, the most typical EP-El Niño, and the distribution of SST anomalies during the winter of 2006/07 was not concentrated over the eastern Pacific but rather widespread in the equatorial central and eastern Pacific. Nevertheless, Yu and Kim (2012) showed that three different definitions of EP- and CP-El Niño all indicate that the 2006/07 event was an EP-El Niño. With *CloudSat/CALIPSO* cloud profile observations, we now have a clear view of three-dimensional cloud structure during the two types of El Niño. This paper has three objectives. First, we aim to provide a thorough depiction of cloud vertical structure changes during the two El Niños, along with large-scale circulation changes. Our analysis results encompass cloud and circulation changes in conventional geographical space and in the functional space of large-scale dynamic regimes, indicated by midtropospheric vertical pressure velocity at 500 hPa ( $\omega_{500}$ ). Second, by contrasting the two events that differ in both SST anomaly magnitude and pattern, we attempt to distinguish the relative roles of SST anomaly magnitude and pattern in determining the tropical cloud and circulation anomalies. Third, we test the representativeness of these two events by placing them in the context of historical El Niños in terms of “strong,” “weak,” “EP,” and “CP” categories and examining whether common features of cloud response exist for each category. The relevance of the results to the general cloud and SST relation is then discussed.

The structure of the paper is as follows. Section 2 describes the data used in the analysis. Section 3 presents

the clouds and circulation anomalies during the two El Niños in geographical space, while section 4 describes cloud changes in the regimes of large-scale circulation and diagnosis of whether the pattern or magnitude of SST anomaly determines the different responses. The TOA cloud forcings for the two events are presented in section 5 and the analysis of historical El Niños is shown in section 6. Concluding remarks are given in section 7.

## 2. Data

The cloud profile data we use include cloud water content (CWC) from *CloudSat* level 2B-CWC-RO and *CloudSat* radar and *CALIPSO* lidar combined cloud fraction retrieval from 2B-GEOPROF-lidar. The vertical resolution of these data is about 500 m, oversampled onto 250-m intervals from the surface to 20 km. The horizontal resolution is 1.7 km along track and 1.3 km cross track. The uncertainty of CWC is about a factor of 2 (Jiang et al. 2012). CWC retrievals within 0.5 km above the surface are not used because of the large uncertainties due to surface clutter. A major limitation of using *CloudSat/CALIPSO* data to examine interannual cloud changes is the short time span of the data record. We construct monthly anomalies relative to the mean seasonal cycle based on the 4-yr data from August 2006 to July 2010. This period includes two warm and two cold episodes of ENSO, making a nearly neutral climatology. To test the representativeness of the anomalies, we compare our *CloudSat/CALIPSO* cloud fraction (CFr) anomalies with satellite records of longer temporal coverage, such as the CFr data from ISCCP, despite the coarse vertical stratification of the latter. We also compare the short-term (August 2006–July 2010) and long-term mean atmospheric circulation (1981–2010) from the interim European Centre for Medium-Range Weather Forecasts (ECMWF) Re-Analysis (ERA-Interim). Given the similarity between such short-term and long-term means, we are assured that the relatively short record of *CloudSat/CALIPSO* observation is useful in studying interannual variabilities.

The ISCCP cloud fraction record used in this study covers the period from July 1983 to December 2009. This version of ISCCP data is the latest release of ISCCP D2 global monthly dataset. The horizontal resolution of the data is  $280\text{ km} \times 280\text{ km}$ . We also use cloud-top pressure measurements from the Moderate Resolution Imaging Spectroradiometer (MODIS) on the *Aqua* satellite to separate low cloud anomalies from anomalies of mid-to-high clouds at low levels. The MODIS data resolution is  $1^{\circ} \times 1^{\circ}$ .

To derive TOA CRF, we use monthly  $1^{\circ} \times 1^{\circ}$  gridded all-sky and clear-sky radiative flux measurements from

CERES on *Terra* and *Aqua* (the SYN1deg-Month-lite edition 2.5-subset data). On the monthly and regional ( $\sim 10^\circ \times 10^\circ$  grid boxes) mean, the CERES shortwave TOA flux bias is less than  $0.2 \text{ W m}^{-2}$ , and the RMS error is between  $0.70$  and  $1.37 \text{ W m}^{-2}$ . For longwave TOA flux, the monthly and regional mean bias is  $0.2\text{--}0.4 \text{ W m}^{-2}$  and the RMS error is less than  $0.7 \text{ W m}^{-2}$  for both *Terra* and *Aqua* CERES (Loeb et al. 2007). These errors originate from the conversion from measured radiances to radiative fluxes and should not be confused with uncertainties of CRF. We define CRF as the difference between the CERES all-sky and clear-sky TOA radiative fluxes, with the positive sign indicating warming of the earth–atmosphere system. This definition has an inherent problem because clear-sky and all-sky measurements do not overlap at each pixel. The difference in atmospheric temperature and humidity between the cloudy and clear-sky scenes would cause errors in CRF, especially for longwave CRF (Soden et al. 2004). To alleviate this problem, we use both the CERES and ERA-Interim clear-sky TOA radiative fluxes in CRF calculations. The difference between the calculations provides an estimate of CRF errors due to atmospheric states.

SST data are from the National Oceanic and Atmospheric Administration (NOAA) optimum interpolation SST, and atmospheric winds are from ERA-Interim with a horizontal resolution of  $1.5^\circ \times 1.5^\circ$ .

### 3. Cloud and circulation changes

As maximum El Niño warming usually occurs in boreal winter, we focus on the cloud and circulation anomalies averaged for December–February (DJF). Figure 1 shows the spatial distributions of SST anomalies relative to the 30-yr mean (1981–2010) climatology for the two El Niños, and the similar anomalies relative to the four DJF means from 2006 to 2010 are shown as insets. In DJF 2009/10, the positive SST anomalies are concentrated between the date line and  $120^\circ\text{W}$ , while the warm anomalies during DJF 2006/07 are widespread across the eastern and central Pacific. The tropical ( $30^\circ\text{S}\text{--}30^\circ\text{N}$ ) averaged SST anomalies are  $0.3^\circ\text{C}$  for DJF 2009/10 and  $0.1^\circ\text{C}$  for DJF 2006/07.

Figure 2 shows the anomalies of tropical ( $30^\circ\text{S}\text{--}30^\circ\text{N}$ ) averaged cloud water content and CFr profiles over the tropical oceans for the four winters, with the tropical mean SST anomalies in each winter displayed in the inset. The tropical averaged cloud anomalies for the two El Niños are almost opposite to each other over most of the troposphere, with an overall reduction of cloudiness in 2009/10 and an increase in 2006/07. At the altitudes above  $14 \text{ km}$  and below  $1.5 \text{ km}$ , both 2009/10 and 2006/07

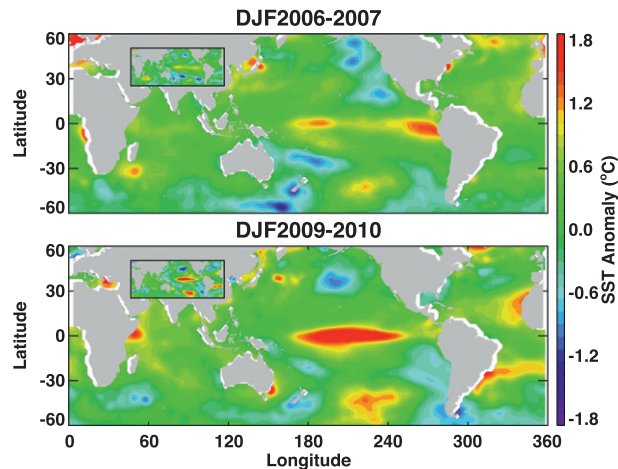


FIG. 1. Horizontal maps of SST anomalies during December–February (DJF) 2006/07 and 2009/10. The anomalies are relative to the 30-yr DJF mean from 1981 to 2010. The anomalies relative to the four DJF means from 2006 to 2010 are shown as insets.

experience an increase of CWC. The changes in CFr are consistent with those in CWC, but are more pronounced for upper tropospheric cirrus clouds because of the higher sensitivity of the lidar to thinner clouds than the radar. The amplitude of the CWC (CFr) anomaly in the tropical average is about  $1 \text{ mg m}^{-3}$  (0.5%). Compared to the 4-yr mean, the fractional difference is up to 5%–10% for CWC and 15%–30% for CFr in the free troposphere (2–14 km). For the two La Niñas, CWC and CFr values between 10 and 12 km are reduced but increased in the middle levels (2–10 km). Below 2 km, 2007/08 experiences a reduction in both CWC and CFr, while 2008/09 has a slightly increased CWC but reduced CFr. Note that the 2008/09 winter was not regarded as a persistent cold episode because the SST anomalies were not over the threshold of  $-0.5^\circ\text{C}$  for a minimum of five consecutive overlapping seasons ([http://www.cpc.ncep.noaa.gov/products/analysis\\_monitoring/ensostuff/ensoyears.shtml](http://www.cpc.ncep.noaa.gov/products/analysis_monitoring/ensostuff/ensoyears.shtml)). If we restrict the spatial averages to the Pacific Ocean only ( $120^\circ\text{E}\text{--}90^\circ\text{W}$ ) (not shown), the cloudiness anomalies are of the same sign, but with smaller amplitude, indicating that the cloud anomalies over the Pacific Ocean are dominant in the tropical average but contributions from other ocean basins are also important (Zhang et al. 1996).

The horizontal distributions of CWC and CFr anomalies at four pressure levels as well as the DJF mean cloud-top pressure from MODIS for the two El Niños are shown in Fig. 3. The four levels represent the planetary boundary layer, the middle and upper troposphere, and the tropopause region. At 900 hPa, the two El Niños exhibit a striking contrast with the cloud anomalies of opposite sign over most of the tropics. In the equatorial

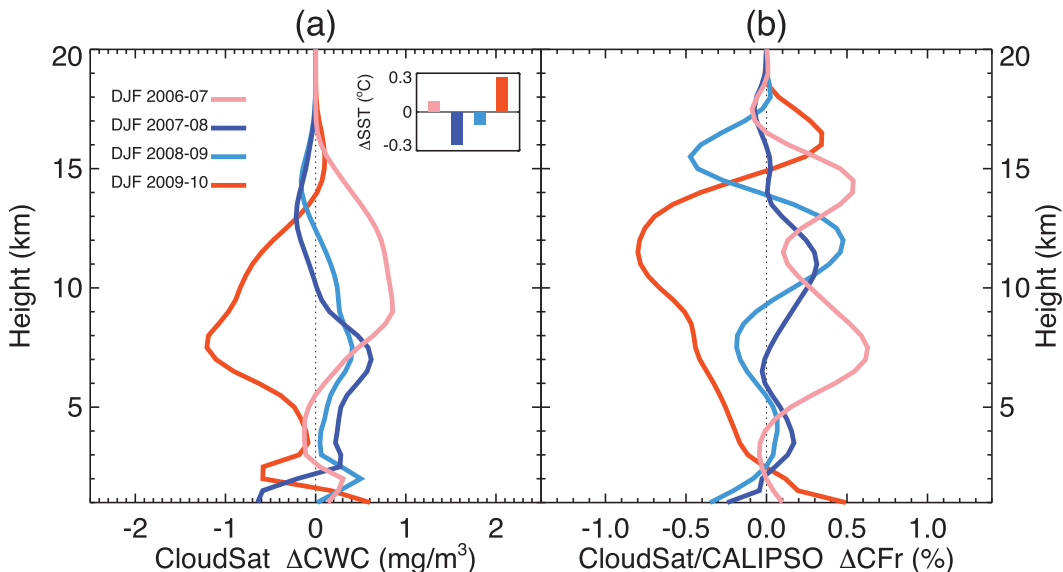


FIG. 2. Tropical-mean anomalies of (left) cloud water content and (right) cloud fraction profiles from *CloudSat/CALIPSO* for the four DJF periods from 2006 to 2009. The anomalies are relative to the four DJF means. Only oceanic regions between  $30^\circ\text{S}$  and  $30^\circ\text{N}$  are averaged. The tropical-mean sea surface temperature anomalies for the four winters are shown in the inset of Fig. 2a.

southeast Pacific, the 2006/07 El Niño produces a decrease of low clouds (identifiable by the high values of MODIS cloud top pressure there), with only a small area of increased low clouds adjacent to the west coast of Peru and Chile. The 2009/10 El Niño, on the contrary, has a strong positive anomaly of low clouds. The magnitude of increased low clouds is about 15% in cloud fraction and  $20 \text{ mg m}^{-3}$  (more than twice the 4-yr mean). Similar changes, but of opposite sign for each event, occur in the southeast Atlantic stratocumulus region. The increase of low cloud amount would have a substantial contribution to the net cloud forcing in the tropics. It may be related to the local negative SST anomalies observed during DJF 2009/10 (see Fig. 1), although it is not clear whether the cold SST anomalies are the consequence of reduced downward solar radiation at the surface associated with the increased low clouds. In the equatorial northeast Pacific (around  $10^\circ\text{N}$ ), the cloud anomalies at 900 hPa are slightly positive in DJF 2006/07 but negative in DJF 2009/10. The MODIS cloud-top pressure indicates that this area lies in a transition zone from low clouds to mid and high clouds. Hence, the cloud anomalies at 900 hPa there could include the changes of stratiform clouds and/or the changes of deep cumulus clouds that penetrate through 900 hPa.

From 600 to 100 hPa, cloud anomalies are approximately barotropic because the changes of deep convective strength dominate the cloud response. The cloud anomalies are substantial at 200 hPa ( $\sim 10 \text{ km}$ ). Interestingly, both El Niños have maximum positive cloud

anomalies near the date line, with the 2009/10 maximum located more toward the south of the equator than the 2006/07 maximum. To the east of the maximum positive cloud anomaly in the Pacific, the two El Niños are more or less similar; however, to the west of the maximum, the two El Niños are drastically different in the middle to upper troposphere (200–600 hPa). Over the western Pacific and Maritime Continent, strong negative high cloud anomalies occur in the winter of 2009/10, compared to the positive high cloud anomalies in DJF 2006/07. Over most of the Indian Ocean, the 2006/07 winter experiences enhanced convection, while the 2009/10 winter shows reduced convection. Opposite cloud anomalies also appear in the equatorial Atlantic Ocean for the two events. At 600 and 100 hPa, cloud anomalies outside the Pacific Ocean are much smaller than those inside the Pacific. During DJF 2009/10, the 100-hPa cloud fraction and CWC anomalies over the Indian and Atlantic Oceans are close to zero but slightly positive, while their counterparts at 200 hPa are negative, suggesting that cirrus variations are not fully determined by changes in deep convection.

The robustness of the *CloudSat/CALIPSO* anomaly pattern is tested in Fig. 4 using the cloud fraction data from ISCCP. We display the ISCCP cloud fraction anomalies for December 2006 and 2009 relative to the December mean based on long-term (1983–2009) and short-term (2006–09) averages. Similar to Clement et al. (2009), we add ISCCP low and middle cloud fraction together because of the uncertainty in the retrieval of

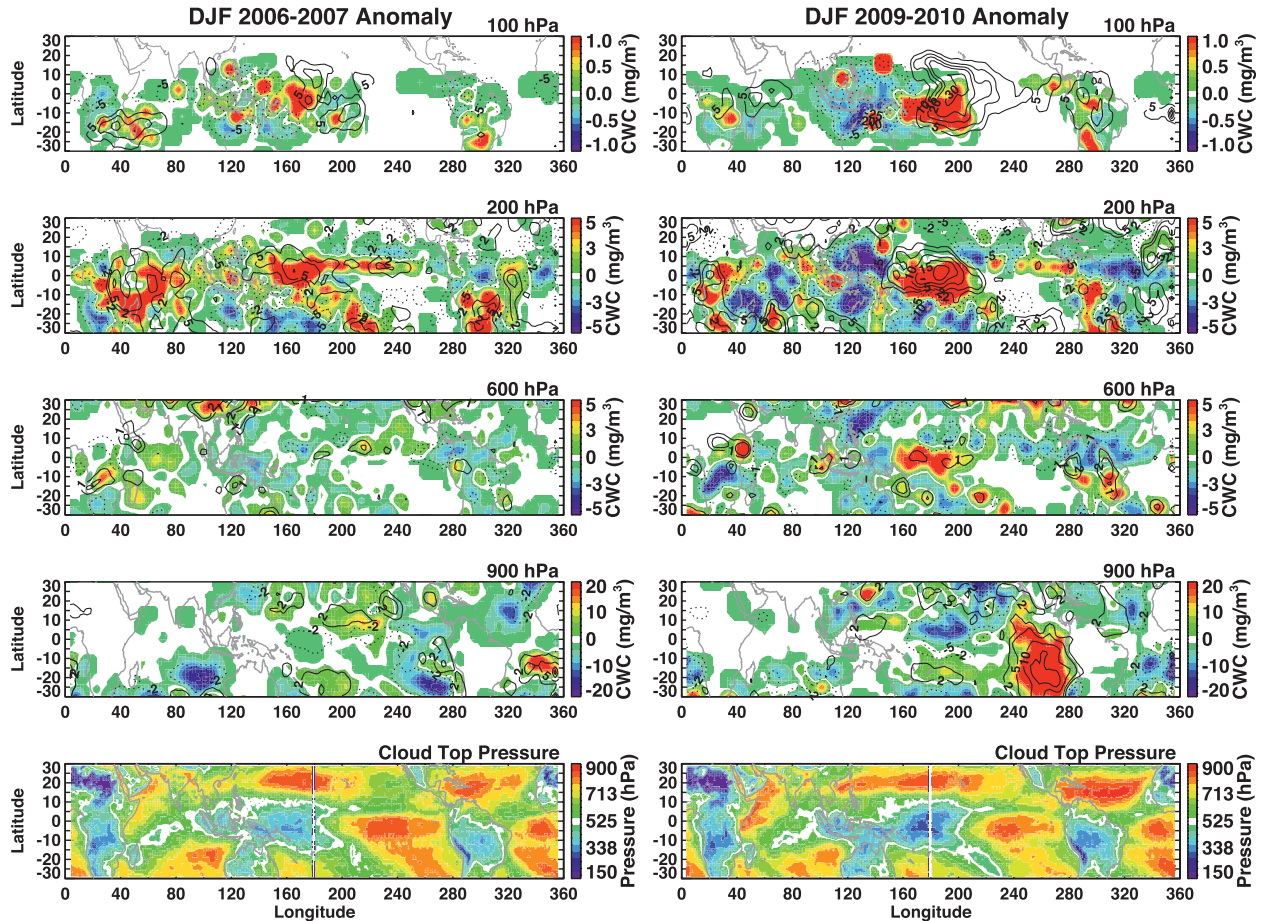


FIG. 3. (top rows) Horizontal maps of cloud anomalies at four vertical levels (cloud water content shown by color shading, cloud fraction by contours) and (bottom row) averaged cloud-top pressure from MODIS for DJF (left) 2006/07 and (right) 2009/10.

low-level cloud-top height. It is clear that the cloud fraction anomalies using different means are very similar. The spatial distributions of cloud fraction anomalies generally agree with those of *CloudSat/CALIPSO*, although it is not meaningful to quantify the differences because of the broad classification of vertical layers in the ISCCP data.

As the changes of tropical cloud anomalies are strongly correlated with changes in tropical circulation, we plot the tropical 3D wind anomalies using the ERA-Interim data together with cloud anomalies from *CloudSat/CALIPSO*. Figure 5 is the longitude–height section for anomalies averaged over 10°S–10°N. Figure 6 is a latitude–height section for zonally averaged anomalies. Only oceanic regions are included in the averages. In both figures, the vertical wind (in  $\text{hPa day}^{-1}$ ) is enlarged 5000 times to stress the overturning circulation.

On the zonal plane (Fig. 5), the 2006/07 El Niño has a widespread increase of mid-to-high clouds across the central and eastern Pacific, but of a small magnitude,

while the 2009/10 El Niño has a much stronger positive deep convective cloud anomaly near the date line. The increase of deep convection is associated with enhanced ascending motions. The high vertical resolution of *CloudSat/CALIPSO* data reveals the fine structure of anomalous cloud profiles that are not available from previous datasets such as the ISCCP. For example, the positive high cloud fraction anomalies above 200 hPa in the central Pacific during DJF 2009/10 exhibit an eastward tilting with height, indicating the role of horizontal winds in advecting detrain ice clouds. During both El Niños, some negative cloud anomalies are underneath or in between moderately strong positive anomalies, creating a rather inhomogeneous response in the vertical. During DJF 2006/07, the compensating subsidence in response to the enhanced ascent is confined within the western Pacific around 90°–135°E, while the 2009/10 El Niño has a far-reaching forced descent beyond the western Pacific, covering most of the Indian (45°–90°E) and Atlantic (300°–360°) Oceans except a narrow range of

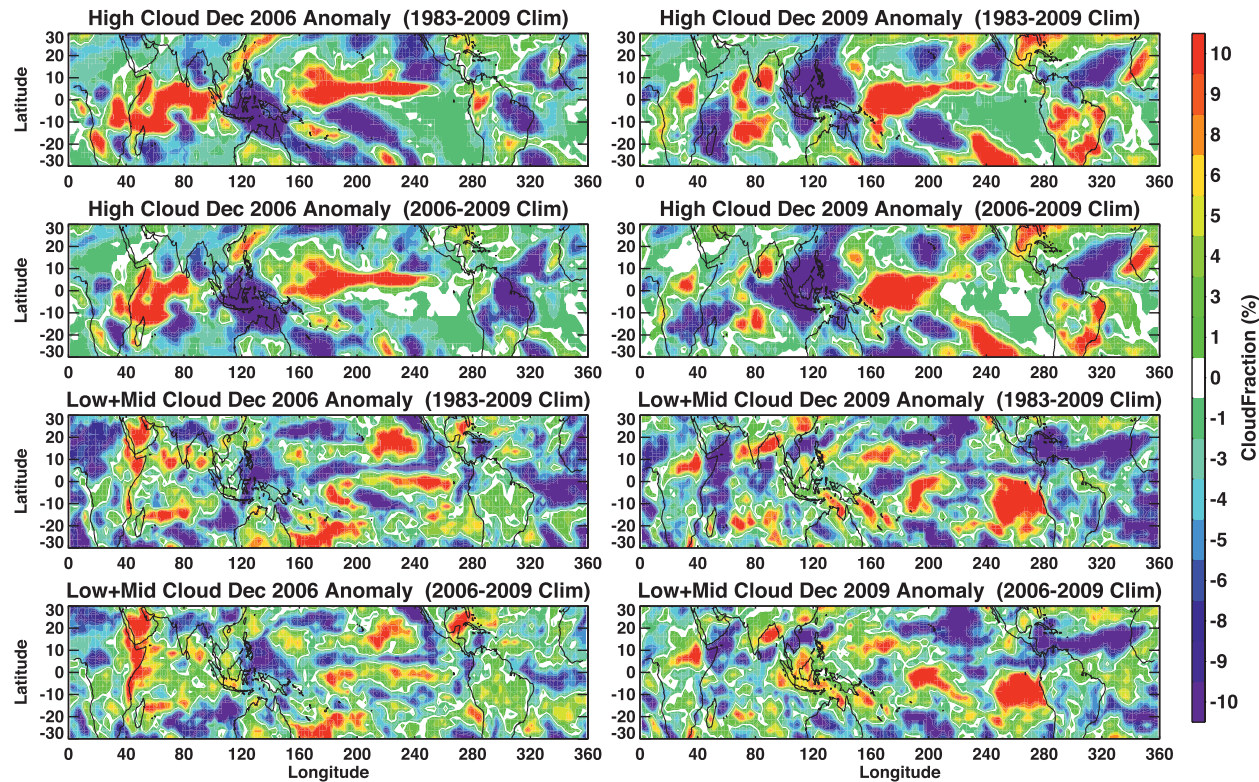


FIG. 4. Horizontal maps of cloud fraction anomalies from ISCCP for December (left) 2006 and (right) 2009. The anomalies in the first and third rows are relative to the mean from 1983 to 2009, while the second and fourth rows are relative to the mean from 2006 to 2009. Middle and low cloud fractions are summed together because of the uncertainty in low cloud-top height identification in the ISCCP data.

longitudes centered around 90°E. Over the Indian Ocean, the two El Niño winters have opposite cloud anomalies although the local SST anomalies are both positive. This is a clear manifestation of the “atmospheric bridge”

(i.e., the remote impact of ENSO SST through atmospheric circulation; Alexander et al. 2002; Su et al. 2001).

On the meridional plane (Fig. 6), the differences between the two El Niños are evident. The 2006/07 El Niño

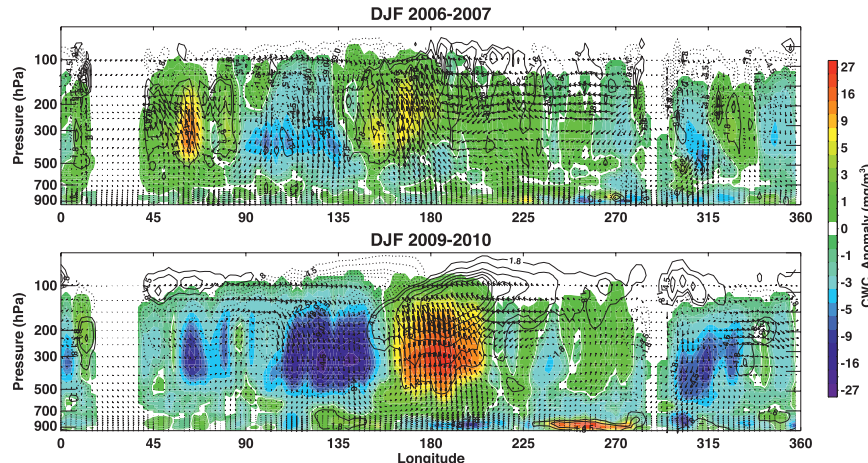


FIG. 5. Longitude–height section of tropical-mean (10°S–10°N) cloud anomalies (cloud water content in shadings, cloud fraction in contours) during DJF 2006/07 and 2009/10, superimposed with ERA-Interim winds. The vertical pressure velocity ( $\text{hPa day}^{-1}$ ) is enlarged 5000 times relative to the horizontal wind ( $\text{m s}^{-1}$ ).

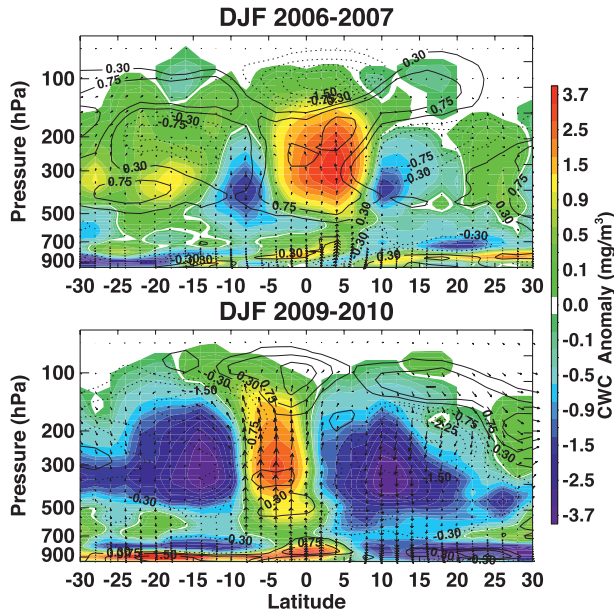


FIG. 6. Latitude–height section of zonal mean ( $0^{\circ}$ – $360^{\circ}$ ) cloud anomalies (cloud water content in shadings, cloud fraction in contours) during DJF 2006/07 and 2009/10, superimposed with ERA-Interim winds. The vertical pressure velocity ( $\text{hPa day}^{-1}$ ) is enlarged 5000 times relative to the horizontal wind ( $\text{m s}^{-1}$ ).

has the maximum anomalous upward motion located to the north of the equator. The compensating subsidence is restricted within  $15^{\circ}$  of the maximum ascending anomaly. Poleward of  $15^{\circ}\text{S}$  and  $20^{\circ}\text{N}$ , circulation anomalies are relatively weak, accompanied by increased middle and high clouds. On the other hand, the 2009/10 El Niño has a maximum of enhanced ascent to the south of the equator. It induces strong descent anomalies poleward of  $10^{\circ}\text{S}$  and  $5^{\circ}\text{N}$ , generating strong negative cloud anomalies. In the boundary layer, clouds anomalies are opposite for the two events, consistent with the large-scale circulation change and probably correlated with the variations of lower tropospheric stability.

#### 4. Cloud changes in the large-scale circulation regimes

Following Bony et al. (2004), we treat tropical cloudiness as a function of  $\omega_{500}$ . In this framework, the tropical mean cloudiness ( $\langle C \rangle$ ) is expressed as an integral of cloudiness in each circulation regime ( $C_{\omega}$ ), weighted by the probability density function (PDF) of each regime ( $P_{\omega}$ ), that is,  $\langle C \rangle = \int_{-\infty}^{+\infty} P_{\omega} C_{\omega} d\omega$ . Thus, the change of tropical mean cloudiness from climatology can be decomposed into a term associated with the change of large-scale circulation (termed the dynamic component),  $C_1 = \int_{-\infty}^{+\infty} \delta P_{\omega} C_{\omega} d\omega$ ; a term associated with the change of cloudiness in each regime

(termed the thermodynamic component),  $C_2 = \int_{-\infty}^{+\infty} P_{\omega} \delta C_{\omega} d\omega$ ; and the covariation between the two,  $C_3 = \int_{-\infty}^{+\infty} \delta P_{\omega} \delta C_{\omega} d\omega$ , where  $\delta P_{\omega}$  and  $\delta C_{\omega}$  are anomalies from their climatological means. Hence, the tropical mean cloud change ( $\delta C$ ) =  $\int_{-\infty}^{+\infty} \delta P_{\omega} C_{\omega} d\omega + \int_{-\infty}^{+\infty} P_{\omega} \delta C_{\omega} d\omega + \int_{-\infty}^{+\infty} \delta P_{\omega} \delta C_{\omega} d\omega$ . We note that the terminologies (dynamic and thermodynamic components) should not be interpreted literally, as the  $C_1$  and  $C_2$  terms are strongly correlated, both being driven by SST anomalies.

Figure 7 shows tropical ( $30^{\circ}\text{S}$ – $30^{\circ}\text{N}$ , ocean only) cloudiness (CWC in color shadings and CFr in line contours) sorted in 20 bins of  $\omega_{500}$  with a bin interval of  $10 \text{ hPa day}^{-1}$  for the two El Niños. Figures 7a and 7b are total cloud amount and Figs. 7c and 7d are cloud anomalies relative to the four DJF means. The three components of cloud anomalies are shown in Fig. 8.

As the SST anomalies are stronger in 2009/10 than in 2006/07, high clouds in the strongly ascending regimes appear higher in altitude and greater in magnitude in both CWC and CFr. The intense high clouds are more concentrated over strongly ascending regimes ( $\omega_{500} < -75 \text{ hPa day}^{-1}$ ) in 2009/10, whereas they span a broader range of ascending regimes in 2006/07 (Figs. 7a,b). The shift to stronger ascending regimes and to higher altitudes in 2009/10 is clearly manifested in the anomalous cloudiness distributions (Figs. 7c,d). The 2009/10 El Niño shows an increase of high clouds in the strongly ascending regime where  $\omega_{500}$  is less than  $-75 \text{ hPa day}^{-1}$ , and a substantial decrease of mid-to-high cloudiness in the moderate circulation regimes, spanning  $\omega_{500}$  between  $-75$  and  $20 \text{ hPa day}^{-1}$  (Fig. 7d). Such a decrease in high and midlevel clouds in the intermediate circulation regimes is a result from the shift of high cloudiness to stronger ascending regime. There is also a decrease of clouds in the boundary layer in the moderate subsidence regimes with  $\omega_{500}$  less than  $20 \text{ hPa day}^{-1}$ . This could be due to the decrease of low clouds themselves and/or the reduction of mid-to-high clouds that span the boundary layer and free troposphere. In the strongly descending regimes with  $\omega_{500}$  between  $20$  and  $60 \text{ hPa day}^{-1}$ , clouds in the boundary layer and middle troposphere are increased. Changes of clouds in the regimes of  $\omega_{500} > 60 \text{ hPa day}^{-1}$  (which are of very small occurrence) are quite small. These cloud anomalies are associated with the changes in the PDF of  $\omega_{500}$  ( $\delta P_{\omega}$ ), which exhibit a polarizing feature: an increase at two extremes and a decrease over the broad range of intermediate  $\omega_{500}$ , corresponding to a strengthened tropical circulation (Fig. 9a). As the moderate  $\omega_{500}$  values ( $-75 < \omega_{500} < 20 \text{ hPa day}^{-1}$ ) account for about 60% of tropical circulation regimes and the relatively large magnitude of cloud anomalies

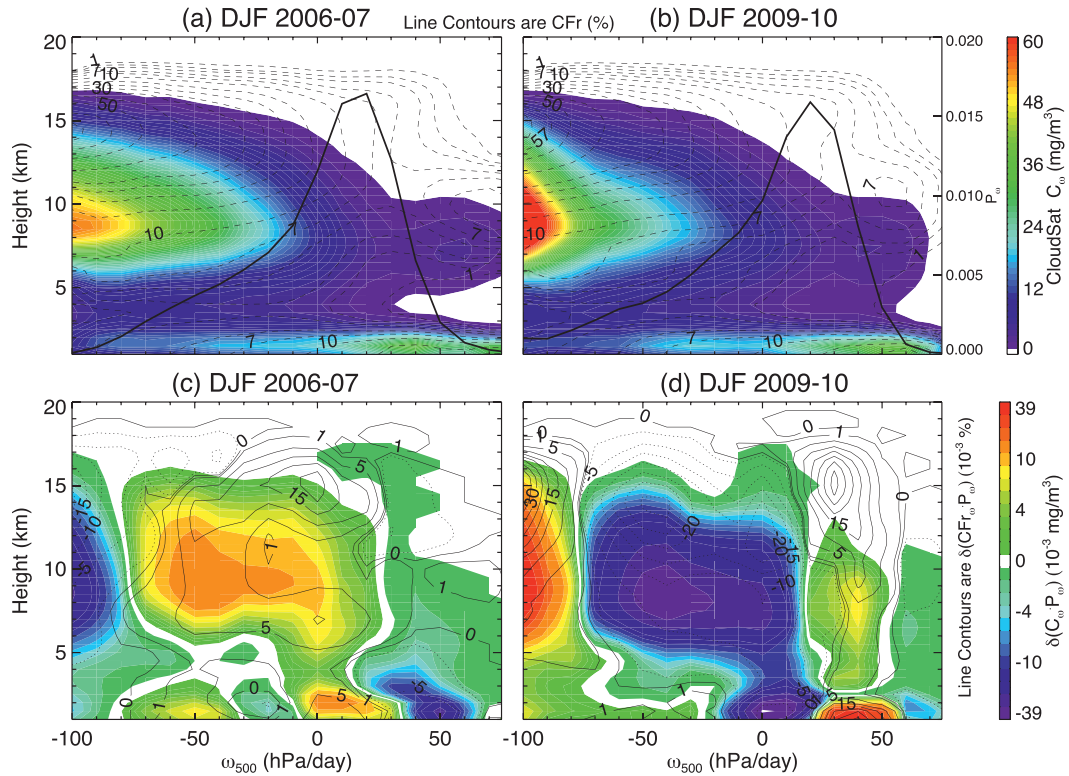


FIG. 7. (a),(b) Tropical clouds and (c),(d) cloud anomalies relative to the four DJF means during the two El Niños sorted as a function of vertical pressure velocity at 500 hPa ( $\omega_{500}$ ). Color shadings indicate cloud water content and contours represent cloud fraction. The solid curves are the (a) 2006/07 and (b) 2009/10 DJF mean probability density functions (PDFs) of  $\omega_{500}$ .

there, the tropical-mean CWC and CFr show a reduction of clouds through most of the troposphere, except below 1 km and above 14 km. The three components ( $C_1$ ,  $C_2$ , and  $C_3$ ) of cloud changes (Figs. 8d–f) indicate that the both dynamic ( $C_1$ ) and thermodynamic ( $C_2$ ) components contribute to the sandwich-like structure in Fig. 7d and that the thermodynamic component ( $C_2$ ) dominates the sum of the three terms. We have also displayed the cloud anomalies in the bins of  $\omega_{500}$  that have equal sample sizes (not shown). In this format, the cloud anomalies in the extreme circulation regimes appear less pronounced than those in Fig. 7d because of the low occurrences; however, the sandwich-like structure is preserved.

On the contrary, during the 2006/07 El Niño, high and middle clouds are reduced over the strongly ascending regimes but increased in the moderate circulation regimes (Fig. 7c), associated with an increase in the PDF of intermediate  $\omega_{500}$  values and a decrease at both extreme ranges, opposite to the 2009/10 El Niño. Hence, the tropical-mean high and middle clouds are increased relative to the 4-yr mean. The changes in the  $\omega_{500}$  PDF indicate a weakening of tropical circulation (Fig. 9a), which resembles climate model simulated circulation

changes in response to uniform SST warming [Bony et al., 2004]. The individual components ( $C_1$  and  $C_2$ ) are largely mirror images of those in 2009/10 but of opposite signs (Figs. 8a–c).

Following Held and Soden (2006), we compute the spatial variance of  $\omega_{500}$  ( $\langle \omega_{500}^{*2} \rangle$ ) over the entire tropics ( $30^{\circ}\text{S}$ – $30^{\circ}\text{N}$ ) and divide it into the zonally symmetric component ( $\langle \omega_{500}^{*2} \rangle$ ) and asymmetric component ( $\langle \omega_{500}'^2 \rangle$ ) to represent the strength of Hadley and Walker circulations, respectively (Fig. 9b); that is,  $\langle \omega_{500}^{*2} \rangle = \langle \omega_{500}^{*2} \rangle + \langle \omega_{500}'^2 \rangle$ . The asterisk, overbar, and prime denote the departure from the tropical mean, the zonal mean, and the departure from the zonal mean, respectively. Note that such definitions of the Hadley and Walker circulation indices are different from other commonly used indices (e.g., Oort and Yienger 1996; Tanaka et al. 2004; Quan et al. 2004; Mitas and Clement 2005) but they form a closed budget for the total spatial variance of  $\omega_{500}$  in the tropics. Thus, the “Hadley circulation” and “Walker circulation” defined here loosely correspond to the mean tropical circulation on the meridional plane and zonal plane, respectively. We find that during DJF 2009/10 the strengthening of the Hadley

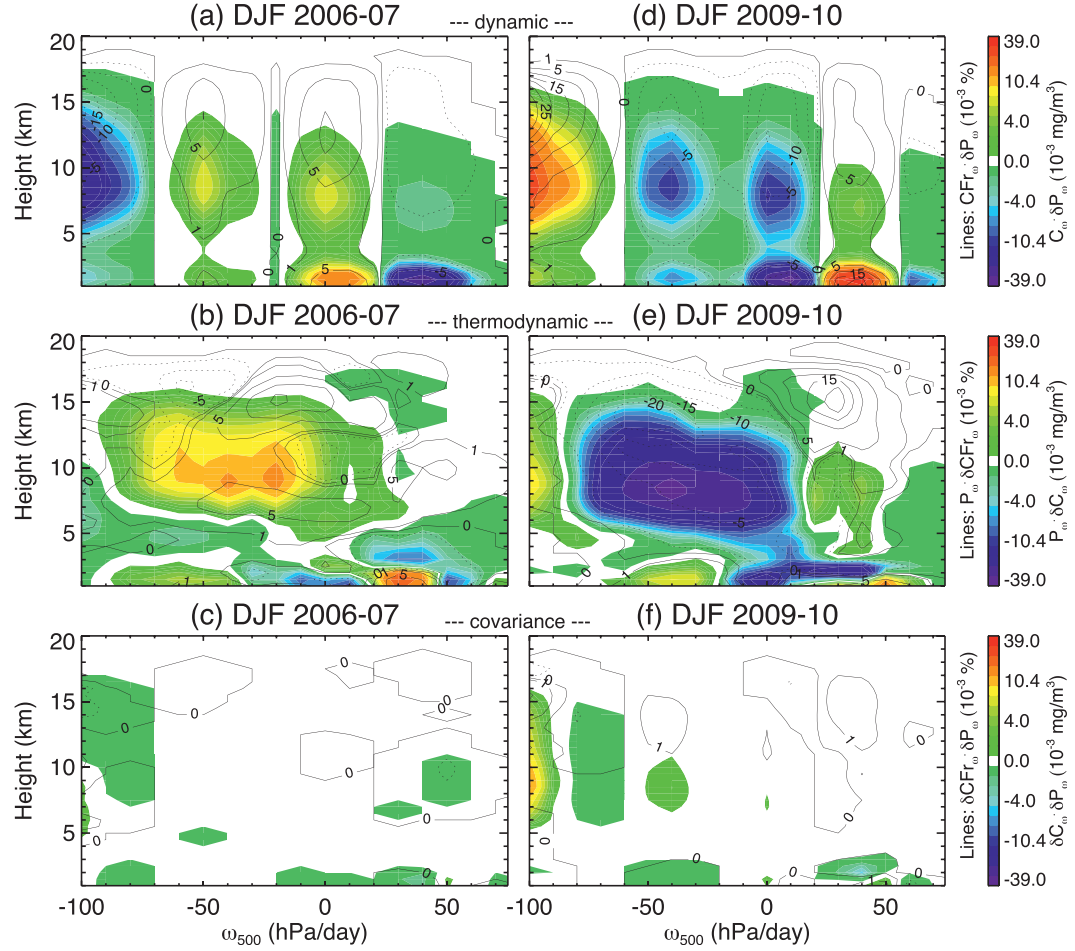


FIG. 8. Three components of the cloud changes as a function of  $\omega_{500}$  for the two El Niños: (a),(d) dynamic component, (b),(e) thermodynamic component, and (c),(f) covariations.

circulation explains 90% of the increased spatial variance of  $\omega_{500}$ , while the rest is contributed by the strengthening of the Walker circulation. During DJF 2006/07, the weakening of circulation is primarily due to the weakening of the Walker circulation, while the weakening of the Hadley circulation accounts for 10% of the decreased spatial variance of  $\omega_{500}$ . For the 2007–08 and 2008–09 La Niñas, the Walker circulation is strengthened but the Hadley circulation is weakened. The changes in the strength of the Hadley and Walker circulations during ENSO have been documented before (Oort and Yienger 1996; Tanaka et al. 2004); however, the changes in the strength of the Hadley and Walker circulations for the two El Niños analyzed here are not inversely correlated as for historical El Niños, indicating the varying nature of El Niños. The anomalies of  $\omega_{500}$  relative to the 30-yr (1980–2010) seasonal mean are similar to the anomalies relative to the 4-yr seasonal mean used here.

What causes the distinctly different responses in clouds and large-scale circulation during the 2009/10 and 2006/07 El Niños? We perform a diagnosis to illustrate the differences in SST anomalies between the two events. Considering that the SST gradient is crucial to determine the tropical circulation and deep convection (Lindzen and Nigam 1987), previous studies (Bony et al. 2004; Williams et al. 2003) suggested that the relative warmth of local SST—that is, the departure of local SST from the tropical-mean SST ( $\delta\text{SST}_i = \text{SST}_i - \langle \text{SST} \rangle$  for the  $i$ th grid box)—correlates better with the local cloud change. We analyze the distributions of  $\delta\text{SST}$  and find that the changes in the occurrence frequency of  $\delta\text{SST}$  in three broadly defined regimes bear approximate similarity to the changes in the PDF of  $\omega_{500}$  (Fig. 10a). During 2009/10, there is an increase in the occurrence of strongly relatively warm SSTs with  $\delta\text{SST} > 2.4^\circ\text{C}$ , approximately the upper ~20% of the  $\delta\text{SST}$  distribution, accompanied by a decrease in the occurrence of

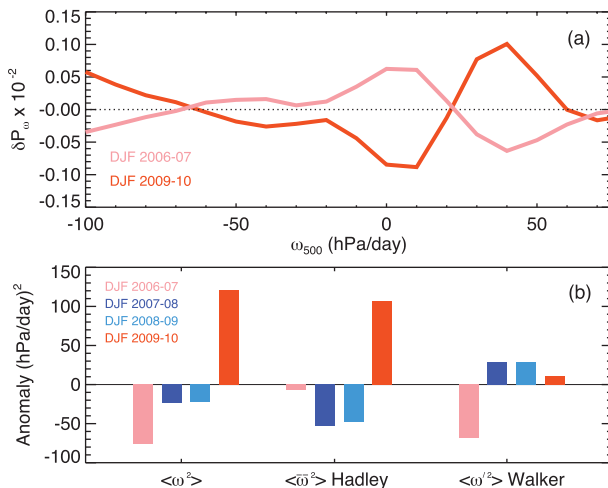


FIG. 9. Changes in tropical circulation during the four DJFs: (a) the changes in the PDF of  $\omega_{500}$  for two El Niños, and (b) the changes in the spatial variances of  $\omega_{500}$ , including zonally symmetric and asymmetric components, for the four DJFs.

intermediate  $\delta\text{SST}$  values (between  $-2.2^\circ$  and  $2.4^\circ\text{C}$ ) and an increase in the occurrence of strongly relatively cold SSTs. The positive SST anomalies during DJF 2006/07 are widespread over the central and eastern Pacific, leading to a reduced SST gradient: the PDF of the extremely relatively warm  $\delta\text{SST}$  decreases and the PDF of the intermediate  $\delta\text{SST}$  increases.

However, the two El Niños also differ in the magnitude of positive SST anomalies. To distinguish the role of SST anomaly magnitude and pattern in determining the  $\delta\text{SST}$  distribution, we keep the spatial distributions of SST anomalies during DJF 2006/07 but enlarge their magnitudes so that the tropical-mean SST anomalies are of the same magnitude for DJF 2006/07 and 2009/10. After this manipulation, the anomaly of  $\delta\text{SST}$  occurrence frequency for 2006/07 changes to a polarized structure, qualitatively similar to that in 2009/10 (Fig. 10b). This exercise suggests that the larger magnitude of SST anomalies during DJF 2009/10 is the key to the strengthened circulation and associated cloud anomalies, although the pattern of SST may also play a role.

## 5. TOA cloud forcings

Given the drastically different cloud anomalies during the two El Niños, it is expected that large differences would occur in their TOA cloud forcings. We analyze TOA CRFs both in the geographical space and in the large-scale circulation regimes. Both CERES and ECMWF clear-sky TOA fluxes are used in conjunction with CERES all-sky TOA fluxes to compute CRF. The spatial maps of longwave, shortwave, and net CRF anomalies from *Terra* CERES as well as the anomalies

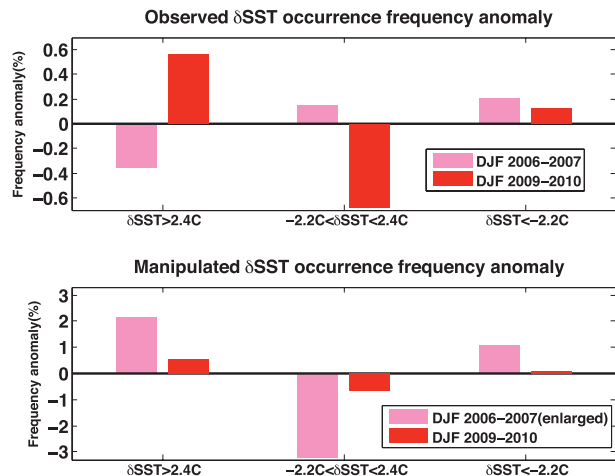


FIG. 10. Changes in the histograms of SST departure from the tropical mean SST for the two El Niños: (top) observed and (bottom) manipulated so that the tropical-mean SST anomalies were the same in DJF 2006/07 and 2009/10. See text for details.

of ratio  $N$  are shown in Fig. 11 and the regime-sorted CRF from *Terra* and *Aqua* CERES and from *Terra* CERES all-sky and ECMWF clear-sky fluxes for both El Niños are shown in Fig. 12. Table 1 summarizes cloud forcing anomalies in different circulation regimes. The anomalies are relative to the four winters from 2006 to 2010. They are similar to the anomalies relative to the 10-yr (8-yr) mean for *Terra* (*Aqua*) CERES data.

The pattern of LWCF anomalies resembles that of cloud anomalies at 200 hPa (Fig. 3), while the shortwave cloud forcing shows combined effects of high, middle, and low cloud anomalies. Interestingly, the net cloud forcing has a similar spatial distribution to the cloud anomalies at 600 hPa, except over the substantial low cloud anomaly regions (i.e., the west coast of South America and Australia). This suggests that middle clouds over convective regions have an important contribution to the net cloud forcing as the LWCF and SWCF from high clouds nearly cancel each other. The ratio  $N$  exhibits appreciable anomalies over regions of relatively large low cloud anomalies, but it has small changes over regions of deep convection such as the western Pacific and the Indian Ocean, indicating the limitation of using this ratio to infer cloud structure changes.

Sorting CRF in the large-scale circulation regimes discloses, to some degree, the contributions of each type of clouds to the total cloud forcing. During DJF 2009/10, the increased deep clouds in the strongest ascending regimes ( $\omega_{500} < -75 \text{ hPa day}^{-1}$ ) produce enhanced shortwave cooling and longwave warming at the TOA, with the shortwave cooling slightly exceeding longwave warming. In the intermediate circulation regimes, the reduction of mid-to-high clouds leads to decreased

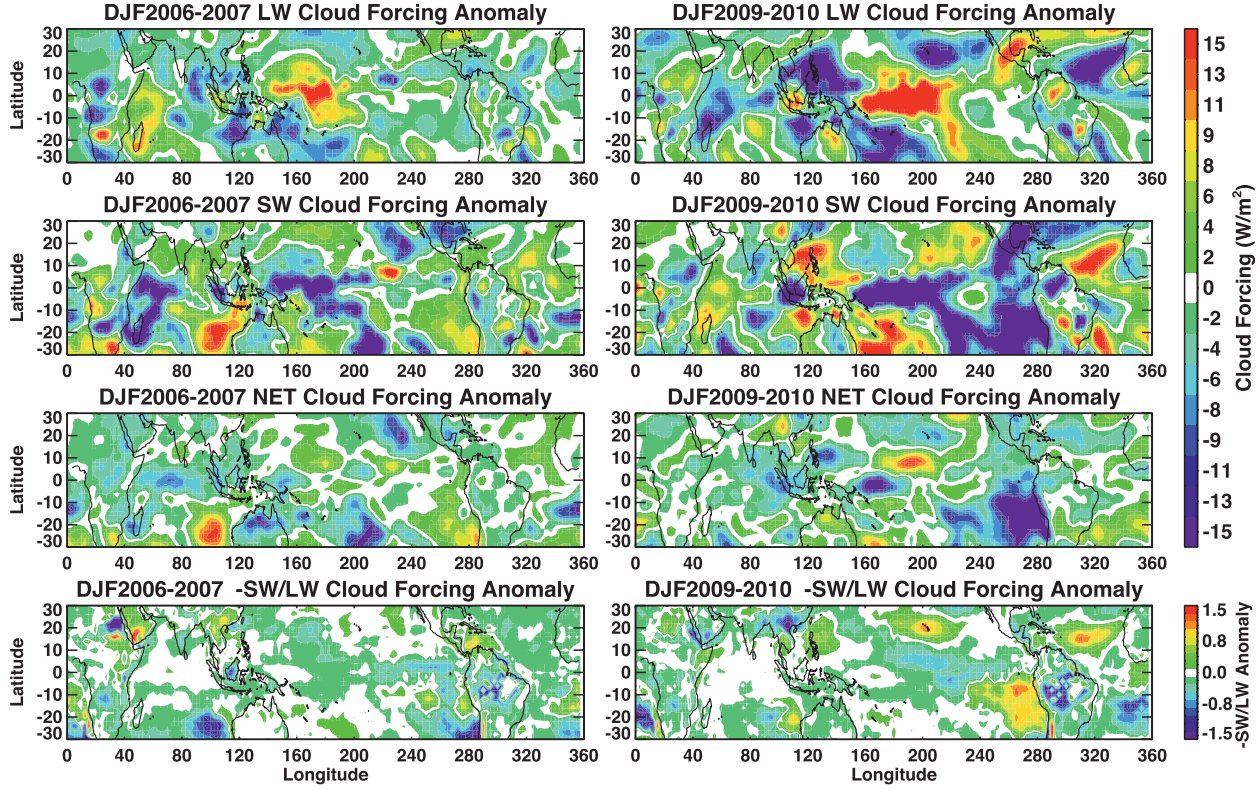


FIG. 11. Horizontal maps of top-of-atmosphere (TOA) cloud forcing anomalies from *Terra* CERES for DJF (left) 2006/07 and (right) 2009/10. (top row) Longwave cloud forcing (LWCF), (second row) shortwave cloud forcing (SWCF), (third row) net cloud forcing, and (bottom row) the ratio  $N = -\text{SWCF/LWCF}$ . The anomalies are relative to the four DJFs from 2006 to 2010. The white areas indicate values of cloud forcing anomalies within  $\pm 0.02 \text{ W m}^{-2}$ , and  $N$  anomalies within  $\pm 0.02$ .

shortwave cooling (positive anomaly) and decreased longwave warming (negative anomaly)—that is, resulting in an anomalous cooling effect. In the strongest descending regimes ( $\omega_{500} > 20 \text{ hPa day}^{-1}$ ), the increased

low cloudiness causes an increased shortwave cooling. The CRF calculated using ECMWF clear-sky fluxes shows similar variations in the regimes of  $\omega_{500}$  to those calculated using CERES clear-sky fluxes, with small

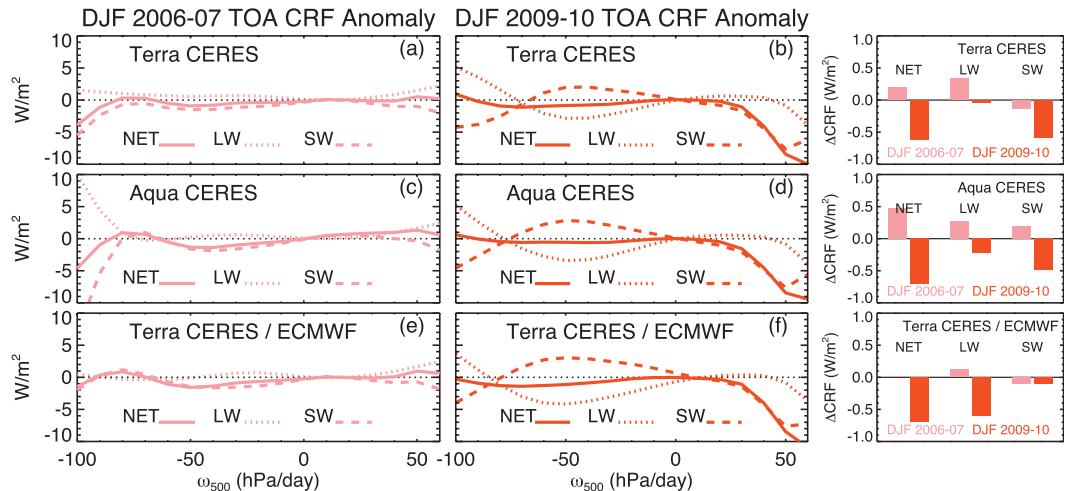


FIG. 12. Changes of TOA cloud forcing as a function of  $\omega_{500}$  for the two El Niños. The tropical-mean TOA net (NET), longwave (LW), and shortwave (SW) CRFs are shown in the rightmost panels. Calculations are made using the radiative flux data from CERES on (top) *Terra* and (middle) *Aqua*, and (bottom) combined *Terra* CERES all-sky and ECMWF clear-sky fluxes.

TABLE 1. The longwave (LW), shortwave (SW), and net (NET) cloud radiative forcing (CRF; in  $\text{W m}^{-2}$ ) anomalies from CERES on *Terra* and *Aqua*, and from the differences between the *Terra* CERES all-sky and ECMWF clear-sky fluxes, averaged for the tropical-mean ( $30^\circ\text{S}$ – $30^\circ\text{N}$ ), and tropical ascending ( $\omega_{500} < 0$ ) and descending ( $\omega_{500} > 0$ ) regimes separately during the 2006/07 and 2009/10 DJF seasons. A positive (negative) sign indicates warming (cooling) of the earth-atmosphere system. The anomalies are relative to the four DJFs from 2006 to 2010.

	2006/07 DJF			2009/10 DJF		
	Tropics	$\omega_{500} < 0$	$\omega_{500} > 0$	Tropics	$\omega_{500} < 0$	$\omega_{500} > 0$
CERES- <i>Terra</i> LW	0.34	0.22	0.12	-0.05	-0.12	0.08
CERES- <i>Terra</i> SW	-0.14	-0.52	0.39	-0.57	-0.07	-0.51
CERES- <i>Terra</i> NET	0.20	-0.30	0.51	-0.62	-0.19	-0.43
CERES- <i>Aqua</i> LW	0.27	0.13	0.14	-0.22	-0.27	0.05
CERES- <i>Aqua</i> SW	0.19	-0.54	0.74	-0.48	0.14	-0.63
CERES- <i>Aqua</i> NET	0.46	-0.41	0.88	-0.70	-0.13	-0.58
CERES- <i>Terra</i> /ECMWF LW	0.12	0.08	0.04	-0.60	-0.55	-0.05
CERES- <i>Terra</i> /ECMWF SW	-0.10	-0.48	0.38	-0.10	0.29	-0.39
CERES- <i>Terra</i> /ECMWF NET	0.02	-0.40	0.42	-0.70	-0.26	-0.44

differences in amplitude. On the tropical average, the net CRFs from all three estimates show a cooling of  $0.6$ – $0.7 \text{ W m}^{-2}$ , to which the cloud changes over the subsidence regimes contribute more than 60% (Table 1). However, the calculations using CERES and ECMWF clear-sky fluxes yield quite different results in longwave and shortwave CRFs separately. Using ECMWF clear-sky fluxes, the net CRF in the tropical mean is dominated by the longwave component, while the net CRF from the calculation using CERES clear-sky fluxes is dominated by the shortwave component. This difference indicates that the influence of atmospheric temperature and moisture on the clear-sky fluxes may be about  $0.5 \text{ W m}^{-2}$  in the tropical mean, with a greater contribution from the large-scale ascending regimes than from the large-scale descending regimes (Table 1).

Compared to DJF 2009/10, DJF 2006/07 shows nearly opposite longwave and shortwave CRF changes in the intermediate circulation regimes ( $-75 < \omega_{500} < 0 \text{ hPa day}^{-1}$ ), consistent with the observed cloud changes. The tropical-mean net CRF anomaly during 2006/07 is  $0.2$ – $0.5 \text{ W m}^{-2}$  warming based on the two CERES datasets and nearly zero ( $0.02 \text{ W m}^{-2}$ ) from the calculation using *Terra* CERES all-sky and ECMWF clear-sky fluxes. The differences between the CERES and ECMWF clear-sky fluxes are larger for the longwave component than for the shortwave component, and the greater differences are seen in the ascending regimes than in the descending regimes as high atmospheric moisture associated with deep convective clouds amplifies the difference between observed clear-sky (between cloud) fluxes and hypothetical clear-sky fluxes for cloudy grid boxes.

The difference in the net CRF at the TOA between the two El Niños are on the order of  $0.7$ – $1.2 \text{ W m}^{-2}$  in the tropical average (Table 1). Such a difference is

significant compared to the CERES TOA flux stability of  $0.5 \text{ W m}^{-2} \text{ decade}^{-1}$  (Loeb et al. 2012). Our analysis suggests that different cloud anomalies in response to the two El Niños can make appreciable perturbations to the net energy balance at the TOA. Our estimates of CRF to ENSO SST warming are of approximately similar magnitude to the previous estimates of  $1$ – $2 \text{ W m}^{-2} \text{ K}^{-1}$  (e.g. Zhang et al. 1996; Zelinka and Hartmann 2011), although the sign may vary from case to case.

## 6. Comparing to the historical El Niños

To compare the two recent El Niños with historical warm episodes, we analyze 27 years (1983–2009) of ISCCP cloud data. Figure 13 shows the tropical-averaged ( $30^\circ\text{S}$ – $30^\circ\text{N}$ , ocean-only) low and middle (low+middle) and high cloud anomalies scattered against tropical-averaged SST anomalies for 27 DJF periods from 1983 to 2009 (December 2009 is used in lieu of the 2009/10 DJF mean because of data availability). The time series of 3-month mean Niño-3.4 ( $5^\circ\text{N}$ – $5^\circ\text{S}$ ,  $170^\circ$ – $120^\circ\text{W}$ ) SST anomalies for this period is displayed in the top panel. We mark the EP- and CP-El Niños based on the consensus classification by Yu and Kim (2012). We also categorize the anomalous warm years into “strong” or “weak” events with the criteria being a DJF mean Niño-3.4 SST anomaly greater than  $1 \text{ K}$  or within  $0.5$ – $1 \text{ K}$ , respectively. The scatterplots for low+middle and high clouds exhibit large scatter with the tropical-mean SST anomalies. The grouping into EP or CP and strong or weak El Niños appears to better align the cloud and SST anomalies; however, there is no simple relation standing out between the tropical-mean cloud and SST anomalies.

The large scatter between the tropical-averaged cloud and SST anomalies highlights the nonlinearity in the

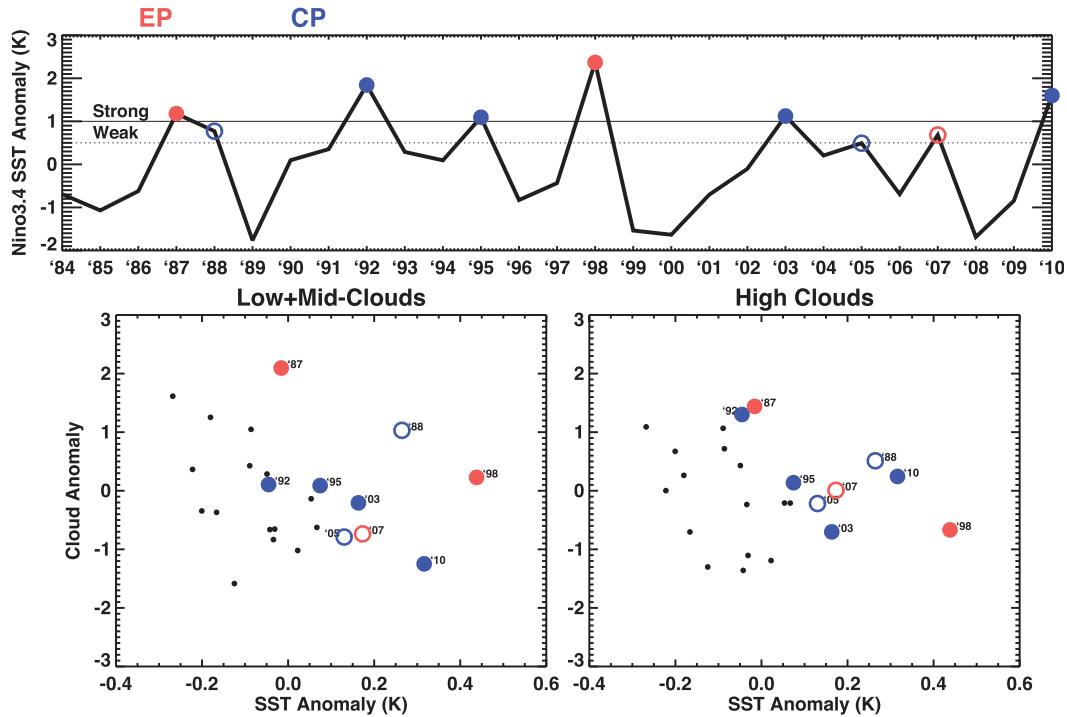


FIG. 13. (top) The time series of DJF averaged Niño-3.4 SST anomalies from 1984 to 2009; (bottom) the DJF averaged tropical-mean ( $30^{\circ}\text{S}$ – $30^{\circ}\text{N}$ ) oceanic cloud anomalies scattered against tropical-mean SST anomalies for (right) low+middle clouds and (left) high clouds from ISCCP. The EP (CP) El Niños are marked by red (blue) color and the solid (open) circles indicate strong (weak) El Niños. See text for details.

ENSO response (Hoerling et al. 1997). Our analysis of the two recent El Niños demonstrates that the nonlinearity stems from the strong coupling of large-scale circulation and convection. As Su and Neelin (2003) pointed out, cloud and precipitation changes are “by-products” of the moist dynamic adjustment to perturbed SST. Hence, it is not surprising that global or tropical mean cloud forcing bears a very weak correlation with the mean surface temperature anomaly on the interannual time scale as shown in Dessler (2010), a characteristic also manifested in tropical-mean precipitation (e.g., Su and Neelin 2003; Gu et al. 2007). However, such nonlinear relation between interannual tropical mean cloud forcing and surface temperature should not be extrapolated to infer long-term cloud climate feedback. On longer time scales (e.g., multidecadal and longer), it is possible that a more linear relation exists between surface temperature change and the overall strength of circulation and convective activity.

## 7. Concluding remarks

With vertically resolved cloud water content and cloud forcing profiles observed by *CloudSat/CALIPSO*, we are able, for the first time, to quantify the vertical

variations of clouds in response to El Niño SST warming. Two El Niños are examined and compared. We conclude that the magnitude and pattern of SST anomalies are both important to the tropical-mean cloud amount change. In the winter of 2009/10, the tropical-mean SST anomaly is about 3 times of that in the winter of 2006/07 and the warmest anomalies are concentrated over the central Pacific, where climatological SST is warm. Consequently, the strong anomalous ascent over the central Pacific moves deep convective clouds higher in altitude and induces a strong descent anomaly remotely, causing a widespread decrease of deep convective clouds in tropical oceans. The zonally overturning circulation (i.e., the Walker circulation) shifts the ascending branch from the western Pacific to the central Pacific and greatly enhances the descending branch to the west (into the Indian Ocean), resulting in little reduction in overall zonal circulation strength as indicated by the zonally asymmetric component of the spatial variance of  $\omega_{500}$ , while the meridionally overturning circulation (i.e., the Hadley circulation) strengthens because of the increased meridional SST gradient. On the other hand, the 2006/07 El Niño is associated with a weakening of the Walker circulation but little change in the Hadley circulation.

Besides large differences in high and middle cloud anomalies, low clouds over the west coast of South America, Australia, and the subtropical Pacific also exhibit nearly opposite responses for the two El Niños. As these low cloud anomalies make a dominant contribution to the net cloud forcing at the TOA, an in-depth analysis of the physical processes responsible for the low cloud change is warranted.

The two El Niños analyzed here exemplify the nonlinear cloud response to surface warming. The relatively longer data record from ISCCP reveals that no simple relation exists for tropical-mean cloud and SST anomalies on interannual time scales. Such a nonlinear cloud response is closely coupled with large-scale circulation changes. As both the magnitude and pattern of SST anomalies come into play in determining the tropical-mean cloud change, it is conceivably difficult for general circulation models (GCMs) to accurately simulate cloud variabilities. GCMs have not yet agreed on the regional scale (a few thousand kilometers; e.g., the central Pacific vs eastern Pacific) surface temperature changes (Merryfield 2006), let alone on the local scale (a few hundred kilometers). The deficiency in capturing regional SST variations, superimposed on the deficiency of model physics in producing clouds at the right time at the right place, presents a great challenge for climate model simulations and predictions. Moreover, the height dependency of cloud response to surface warming and the uniqueness of individual El Niños accentuate the importance of continued global measurements of three-dimensional cloud structure from space.

**Acknowledgments.** We thank T. J. Shen for help with data analysis and thank G. Stephens, J. D. Neelin, and K. Minschwaner for helpful discussions. We appreciate thoughtful comments from three anonymous reviewers. We are especially grateful to D. Vane for funding support. This work was performed at Jet Propulsion Laboratory, California Institute of Technology, under contract with NASA.

## REFERENCES

- Alexander, M. A., I. Bladé, M. Newman, J. R. Lanzante, N.-C. Lau, and J. D. Scott, 2002: The atmospheric bridge: The influence of ENSO teleconnections on air-sea interaction over the global oceans. *J. Climate*, **15**, 2205–2231.
- Allan, R. P., A. Slingo, and M. A. Ringer, 2002: Influence of dynamics on the changes in tropical cloud radiative forcing during the 1998 El Niño. *J. Climate*, **15**, 1979–1986.
- Ashok, K., S. K. Behera, S. A. Rao, H. Weng, and T. Yamagata, 2007: El Niño Modoki and its possible teleconnection. *J. Geophys. Res.*, **112**, C11007, doi:10.1029/2006JC003798.
- Bony, S., J.-L. Dufresne, H. LeTreut, J.-J. Morcrette, and C. Senior, 2004: On dynamic and thermodynamic components of cloud changes. *Climate Dyn.*, **22**, 71–86.
- Cess, R. D., M. Zhang, B. A. Wielicki, D. F. Young, X. Zhou, and Y. Nikitenko, 2001: The influence of the 1998 El Niño upon cloud-radiative forcing over the Pacific warm pool. *J. Climate*, **14**, 2129–2137.
- Clement, A. C., R. Burgman, and J. R. Norris, 2009: Observational and model evidence for positive low-level cloud feedback. *Science*, **325**, 460–464, doi:10.1126/science.1171255.
- Dessler, A., 2010: A determination of the cloud feedback from climate variations over the past decade. *Science*, **330**, 1523–1527.
- Gu, G., R. F. Adler, G. J. Huffman, and S. Curtis, 2007: Tropical rainfall variability on interannual-to-interdecadal and longer time scales derived from the GPCP monthly product. *J. Climate*, **20**, 4033–4046.
- Held, I. M., and B. J. Soden, 2006: Robust responses of the hydrological cycle to global warming. *J. Climate*, **19**, 5686–5699.
- Hoerling, M. P., A. Kumar, and M. Zhong, 1997: El Niño, La Niña, and the nonlinearity of their teleconnections. *J. Climate*, **10**, 1769–1786.
- Jiang, J. H., and Coauthors, 2012: Evaluation of cloud and water vapor simulations in CMIP5 climate models using NASA “A-Train” satellite observations. *J. Geophys. Res.*, **117**, D1410, doi:10.1029/2011JD017237.
- Kao, H.-Y., and J.-Y. Yu, 2009: Contrasting eastern-Pacific and central-Pacific types of ENSO. *J. Climate*, **22**, 615–632.
- Kim, H., P. J. Webster, and J. A. Curry, 2009: Impact of shifting patterns of Pacific Ocean warming on North Atlantic tropical cyclones. *Science*, **325**, 77–80, doi:10.1126/science.1174062.
- Kug, J.-S., F.-F. Jin, and S.-I. An, 2009: Two types of El Niño events: Cold tongue El Niño and warm pool El Niño. *J. Climate*, **22**, 1499–1515.
- Latif, M., R. Kleeman, and C. Eckert, 1997: Greenhouse warming, decadal variability, or El Niño? An attempt to understand the anomalous 1990s. *J. Climate*, **10**, 2221–2239.
- Lee, T., and M. J. McPhaden, 2010: Increasing intensity of El Niño in the central-equatorial Pacific. *Geophys. Res. Lett.*, **37**, L14603, doi:10.1029/2010GL044007.
- Lindzen, R. S., and S. Nigam, 1987: On the role of sea surface temperature gradients in forcing low-level winds and convergence in the tropics. *J. Atmos. Sci.*, **44**, 2418–2436.
- Loeb, N. G., and Coauthors, 2007: Angular distribution models for top-of-atmosphere radiative flux estimation from the Clouds and the Earth’s Radiant Energy System Instrument on the *Terra* satellite. Part II: Validation. *J. Atmos. Oceanic Technol.*, **24**, 564–584.
- , S. Kato, W. Su, T. Wong, F. G. Rose, D. R. Doelling, J. R. Norris, and X. Huang, 2012: Advances in understanding top-of-atmosphere radiation variability from satellite observations. *Surv. Geophys.*, **33**, 359–385, doi:10.1007/s10712-012-9175-1.
- Merryfield, W. J., 2006: Changes to ENSO under CO<sub>2</sub> doubling in a multimodel ensemble. *J. Climate*, **19**, 4009–4027.
- Mitas, C. M., and A. Clement, 2005: Has the Hadley cell been strengthening in recent decades? *Geophys. Res. Lett.*, **32**, L03809, doi:10.1029/2004GL021765.
- Oort, A. H., and J. J. Yienger, 1996: Observed interannual variability in the Hadley circulation and its connection to ENSO. *J. Climate*, **9**, 2751–2767.
- Quan, X. W., and Coauthors, 2004: Change of the tropical Hadley cell since 1950. *The Hadley Circulation: Past, Present, and Future*, H. F. Diaz and R. S. Bradley, Eds., Cambridge University Press, 85–120.
- Ramanathan, V., and W. Collins, 1991: Thermodynamic regulation of ocean warming by cirrus clouds deduced from observations of the 1987 El Niño. *Nature*, **351**, 27–32.

- Soden, J. B., A. J. Broccoli, and R. S. Hemler, 2004: On the use of cloud forcing to estimate cloud feedback. *J. Climate*, **17**, 3661–3665.
- Su, H., and J. D. Neelin, 2003: The scatter in tropical average precipitation anomalies. *J. Climate*, **16**, 3966–3977.
- , —, and C. Chou, 2001: Tropical teleconnection and local response to SST anomalies during the 1997–1998 El Niño. *J. Geophys. Res.*, **106** (D17), 20 025–20 043.
- Tanaka, H. L., and Coauthors, 2004: Trend and interannual variability of Walker, monsoon and Hadley circulations defined by velocity potential in the upper troposphere. *Tellus*, **56**, 250–269.
- Weng, H., K. Ashok, S. K. Behera, S. A. Rao, and T. Yamagata, 2007: Impacts of recent El Niño Modoki on dry/wet conditions in the Pacific rim during boreal summer. *Climate Dyn.*, **29**, 113–129.
- , S. K. Behera, and T. Yamagata, 2009: Anomalous winter climate conditions in the Pacific rim during recent El Niño Modoki and El Niño events. *Climate Dyn.*, **32**, 663–674.
- Williams, K. D., M. A. Ringer, and C. A. Senior, 2003: Evaluating the cloud response to climate change and current climate variability. *Climate Dyn.*, **20**, 705–721.
- Yeh, S.-W., J.-S. Kug, B. Dewitte, M.-H. Kwon, B. Kirtman, and F.-F. Jin, 2009: El Niño in a changing climate. *Nature*, **461**, 511–514, doi:10.1038/nature08316.
- Yu, J.-Y., and S. T. Kim, 2012: Identifying the types of major El Niño events since 1870. *Int. J. Climatol.*, doi:10.1002/joc.3575, in press.
- Yuan, J., D. L. Hartmann, and R. Wood, 2008: Dynamic effects on the tropical cloud radiative forcing and radiation budget. *J. Climate*, **21**, 2337–2351.
- Zelinka, M. D., and D. L. Hartmann, 2011: The observed sensitivity of high clouds to mean surface temperature anomalies in the tropics. *J. Geophys. Res.*, **116**, D23103, doi:10.1029/2011JD016459.
- Zhang, M. H., R. D. Cess, and S. C. Xie, 1996: Relationship between cloud radiative forcing and sea surface temperatures over the entire tropical oceans. *J. Climate*, **9**, 1374–1384.